Autonomous Robots manuscript No.
(will be inserted by the editor)

Optimal Solution of the Generalized Dubins Interval Problem

Finding the Shortest Curvature-constrained Path Through a Set of Regions

Petr Váňa · Jan Faigl

Received: date / Accepted: date

Abstract The Generalized Dubins Interval Problem (GDIP) stands to determine the minimal length path connecting two disk-shaped regions where the departure and terminal headings of Dubins vehicle are within the specified angle intervals. The GDIP is a generalization of the existing point-to-point planning problem for Dubins vehicle with a single heading angle per particular location that can be solved optimally using closed-form expression. For the GDIP, both the heading angles and locations need to be chosen from continuous sets which makes the problem challenging because of infinite possibilities how to connect the regions by Dubins path. We provide the optimal solution of the introduced GDIP based on detailed problem analysis. Moreover, we propose to employ the GDIP to provide the first tight lower bound for the Dubins Touring Regions Problem (DTRP) which stands to find the shortest curvature-constrained path through a set of regions in the prescribed order.

Keywords Dubins vehicle · Multi-goal planning · Generalized Dubins Interval Problem · Dubins Touring Regions Problem

1 Introduction

Surveillance missions are frequent tasks for unmanned aerial vehicles in which the vehicles are requested to visit a given set of target locations and collect the required data. If the sequence of visits to the locations is known a priori, the problem can be formulated as the *Dubins Touring Problem* (DTP) Faigl et al. (2017) in which the movement of the vehicle is restricted by the motion constraints of Dubins vehicle (Dubins, 1957). Thus, a solution of the DTP is the shortest curvature-constrained multi-goal path connecting the requested target locations in the prescribed order.

Moreover, a target location can be considered visited if the vehicle is within a specified distance from it, e.g., using remote data collection or range measurements, and we formulate the problem as the *Dubins Touring Regions Problem* (DTRP). The solution of the problem is described by visiting locations to the given regions and the corresponding heading angles. The final path is constructing by the shortest curvature-constrained segments for Dubins vehicle. Thus, the DTRP is a continuous optimization problem for which the visiting locations and heading angles are selected such that the length of the final path is minimized. However, the optimization of locations and headings cannot be separated without loss of optimality because both parts are tightly coupled.

The DTRP is often studied in the literature in its extended variant called the *Dubins Traveling Salesman Problem with Neighborhoods* (DTSPN) (Obermeyer, 2009) in which the sequence of visits is not known a priori, and thus the problem also contains a combinatorial part. Existing approaches, originally developed for the DTSPN, can also be applied for the DTRP, and therefore, a brief overview of the approaches for the related DTSPN is provided in the following text.

Two main groups of the approaches to the DTSPN can be found in the literature (Macharet and Campos, 2018): sampling-based and decoupled approaches.

The presented work has been supported by the Czech Science Foundation (GAČR) under research project No. 19-20238S.

Petr Váňa and Jan Faigl
Dept. of Computer Science, Faculty of Electrical Engineering, Czech Technical University in Prague, Technická 2
166 27 Prague, Czech Republic
E-mail: {vanapet1,faiglj}@fel.cvut.cz

Sampling-based methods discretize the continuous domains of the headings and locations and employ existing routing solvers (Oberlin et al., 2010) to find heuristic or even optimal solution, but only of the Discretized Dubins TSP (Cohen et al., 2017). In the decoupled approaches, the combinatorial sequencing part is addressed independently on the continuous optimization, e.g., using a solution of the Euclidean TSP (Savla et al., 2005; Macharet et al., 2011; Yu and Hung, 2012; Isaacs et al., 2011). Then, for a given sequence of visits to the target regions, the problem can be called the *Dubins Touring Problem* (DTP) to distinguish its focus on determining the optimal headings at the waypoint locations (Faigl et al., 2017).

Savla et al. (2005) address the DTSP by the decoupled heuristic approach and the authors show that solutions provided by their Alternating Algorithm are proved to be bounded by the solution of the Euclidean TSP; however, the gap to the optimal solution is not tight, and it provides only a rough estimation of the solution quality. An approximation algorithm for the DTSP proposed by Le Ny et al. (2007) improves the worst found solution, especially for high-density instances, but the bound is still impractically high. A special case of the DTP with target locations that are more than four times of the minimum turning radius apart is addressed by Goaoc et al. (2013). The authors show that such constrained DTP is reducible to a finite number of convex optimization sub-problems that can be bounded by 2^{2n-2} for n locations in the sequence, which is however computationally challenging.

The major step towards the optimal solution of the DTRP has been made by Manyam et al. (2017) who provided the first tight estimation of the solution quality of the DTP by introducing the *Dubins Interval Problem* (DIP). The DIP is a generalization of the point-to-point trajectory planning where the departure and terminal headings of Dubins vehicle are prescribed not as a single heading value, but as an interval. Based on the DIP, (Manyam and Rathinam, 2018) have proposed a tight lower bound of the DTSP.

In (Faigl et al., 2017), the optimal solution of the DIP is employed to quickly find high-quality solutions of the DTP by steering sampling of the possible heading values, e.g., finding solutions for a sequence of 50 target locations with the path length less than 1 % from the optima in less than 10 seconds. Here, it is worth noting that an efficient solution of the DTP enables solving other Dubins routing problems like the Dubins Orienteering Problem (Pěnička et al., 2017), where many sequences of subsets of the targets need to be evaluated.

The optimal solution of the DIP (Manyam et al., 2017) and high-quality solutions of the DTP with tight bounds on its quality (Faigl et al., 2017) are the fundamental building blocks to address the DTRP and they represent a systematical way to analyze the problem. However, the DIP cannot be directly utilized for similar insights to the DTRP because of lack of the particular endpoints in the prescribed regions. Therefore, motivated by the achievements enabled by the optimal solution of the DIP, we introduce the **Generalized Dubins Interval Problem** (GDIP) to find the shortest Dubins path between two regions with heading angles at the endpoints constrained to the prescribed continuous intervals as in the DIP, see Fig. 1 with an instance of the GDIP.

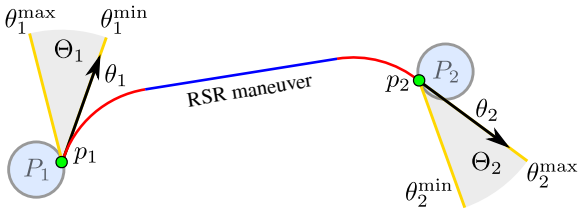

Fig. 1 GDIP instance $(P_1, \Theta_1, P_2, \Theta_2)$ and its solution that connects the regions P_1 and P_2 using the departure angle $\theta_1 \in \Theta_1$ and the terminal angle $\theta_2 \in \Theta_2$ at the particular locations $p_1 \in P_1$ and $p_2 \in P_2$.

Based on the theoretical analysis of the GDIP, we find its optimal solution. Then, we employ the optimal solution of the GDIP to establish the first tight lower bound algorithm for the DTRP. The lower bound not only bounds the length of the optimal solution, but it also steers the searching procedure of finding a high-quality solution of the DTRP. The main contributions are considered as follows:

1. The introduction of the Generalized Dubins Interval Problem (GDIP).
2. The reduction of the GDIP instances to its One-Sided version (OS-GDIP).
3. The optimal solution of the GDIP based on the transformation to the OS-GDIP.
4. The first tight lower bound of the DTRP.
5. Efficient sampling-based algorithm to iteratively reduce the relative gap between the lower bound and a feasible solution of the DTRP.

The rest of the paper is organized as follows. A brief description of the DIP and its properties is presented in the following section, because it is an important part of the background for the proposed approach. The proposed GDIP is introduced in Section 3 and its transformation to the One-Sided GDIP (OS-GDIP) is presented in Section 4 with the proof of its correctness. The optimal solution of the GDIP is presented in Section 5. The proposed deployment of the GDIP in the lower bound and feasible solution of the DTRP is presented

in Section 6. Empirical evaluation of the real computational requirements are reported in Section 7 together with the evaluation of the proposed GDIP deployment in the DTRP. The concluding remarks are in Section 8.

2 Dubins Vehicle and Dubins Interval Problem

Dubins vehicle is a curvature-constrained model defined by the constant forward speed v and the minimum turning radius ρ. The state of the vehicle $q \in SE(2)$ is given by its position $p = (x, y)$ and heading angle $\theta \in \mathbb{S}^1$. The motion model can be expressed as

$$\dot{q} = \begin{bmatrix} \dot{x} \\ \dot{y} \\ \dot{\theta} \end{bmatrix} = v \begin{bmatrix} \cos\theta \\ \sin\theta \\ \frac{u}{\rho} \end{bmatrix}, \quad |u| \leq 1, \tag{1}$$

where u is the control input.

The closed-form solution of the shortest path between two configurations $q_1, q_2 \in SE(2)$ has been found by Dubins (1957), and thus it is called Dubins maneuver. The maneuver is a combination of up to three straight (S) and arc (C) segments with the radius ρ, which results in two basic types of the maneuvers: CSC and CCC. The maneuver length is a piecewise continuous function with discontinuities at the boundary between these two basic maneuver types, and the transition may occur only if the endpoints are closer than four times ρ (denoted as D_4) (Bui et al., 1994); otherwise, the CCC cannot be constructed.

The *Dubins Interval Problem* (DIP) is a problem to find the shortest Dubins maneuver from the state $q_1 = (p_1, \theta_1)$ to $q_2 = (p_2, \theta_2)$ such that the locations p_1 and p_2 are fixed but the heading angles θ_1 and θ_2 are from the specified closed interval $\theta_1 \in \Theta_1$ and $\theta_2 \in \Theta_2$.

Problem 1 (DIP)

$$\min_{\theta_1,\theta_2} \mathcal{L}((p_1,\theta_1),(p_2,\theta_2)),$$
$$\text{s.t.} \quad \theta_1 \in \Theta_1,\ \theta_2 \in \Theta_2,$$

where $\mathcal{L}(\cdot,\cdot)$ is the length of Dubins maneuver between two configurations of the vehicle.

The DIP has been introduced by Manyam et al. (2017), and the authors utilized the Pontryagin's minimum principle to prove the necessary conditions for the optimal solution. These conditions are summarized in Table 1 and the maneuvers can be divided into nine cases. In this paper, we follow the original notation in which $\theta_i^{\min}$ and $\theta_i^{\max}$ is the rightmost and leftmost heading angle of the particular interval, respectively. An orientation of the turns is distinguish by L (left) and R (right), and the subscript C_ψ denotes the angle of the turn is greater than π.

Table 1 List of all possibly optimal solutions of the DIP with its necessary conditions for the terminal and departure angles proposed first by Manyam et al. (2017)

Case	Maneuvers		Conditions on θ_1 and θ_2
1)	S or L_ψ or R_ψ [1]		
2)	LS or LR_ψ	for	$\theta_1 = \theta_1^{\max}$ and $\theta_2 \in \Theta_2$
3)	RS or RL_ψ	for	$\theta_1 = \theta_1^{\min}$ and $\theta_2 \in \Theta_2$
4)	SL or $R_\psi L$	for	$\theta_1 \in \Theta_1$ and $\theta_2 = \theta_2^{\min}$
5)	SR or $L_\psi R$	for	$\theta_1 \in \Theta_1$ and $\theta_2 = \theta_2^{\max}$
6)	LSR	for	$\theta_1 = \theta_1^{\max}$ and $\theta_2 = \theta_2^{\max}$
7)	LSL or $LR_\psi L$	for	$\theta_1 = \theta_1^{\max}$ and $\theta_2 = \theta_2^{\min}$
8)	RSL	for	$\theta_1 = \theta_1^{\min}$ and $\theta_2 = \theta_2^{\min}$
9)	RSR or $RL_\psi R$	for	$\theta_1 = \theta_1^{\min}$ and $\theta_2 = \theta_2^{\max}$

Based on the necessary conditions for the optimal solution of the DIP, the shortest path can be constructed separately for each particular case, if it exists. Then, the final solution is selected as the shortest one. Importantly, there exists a closed-form expression for each particular case, because the first case contains only a single segment and at least one heading angle is fixed for the remaining types.

The DIP is a crucial building block for developing algorithms for more complex problems. Manyam et al. (2017) have used the DIP for a tight lower bound estimation of the DTP. The main idea is based on dividing possible headings at the target locations into a set of heading intervals and transforming the problem into finding the shortest tour on the discrete graph where particular distances are found as the solution of the corresponding instances of the DIP. In (Faigl et al., 2017), the lower bound based on the DIP is employed in the Iteratively-Refined Informed Sampling (IRIS) of the heading intervals to support a quick convergence of the solution to the lower bound. The primary motivation behind the proposed GDIP is to achieve similar results also for Dubins path visiting a sequence of target regions, here, formulated as the DTRP.

3 The Generalized Dubins Interval Problem

The **Generalized Dubins Interval Problem** (GDIP) can be defined as follows. Let P_1, P_2 be compact regions in $\mathbb{R}^2$ and Θ_1, Θ_2 be closed intervals in $\mathbb{S}^1$. The GDIP stands to find the shortest Dubins maneuver from P_1 to P_2 such that the heading angles are within the specified closed intervals Θ_1 and Θ_2, respectively.

[1] $L_\psi R_\psi$ and $R_\psi L_\psi$ types are claimed by Manyam et al. (2017) to be candidates to the optimal solution of the DIP, but they are not local minima. A formal proof is provided in Appendix A.

Problem 2 (GDIP)

$$\min_{p_1,\theta_1,p_2,\theta_2} \mathcal{L}((p_1,\theta_1),(p_2,\theta_2)),$$
$$\text{s.t. } p_1 \in P_1,\ \theta_1 \in \Theta_1,\ p_2 \in P_2,\ \theta_2 \in \Theta_2,$$

where $\mathcal{L}(\cdot,\cdot)$ is the length of the corresponding Dubins maneuver connecting two configurations of the vehicle.

In general, the regions P_1, P_2 can be of any shape but in the rest of this paper, the regions are restricted to the disks with the radii r_1 and r_2 centered at c_1 and c_2, respectively. Thus, for the endpoints $p_1 \in P_1$ and $p_2 \in P_2$, it holds

$$\|p_1 - c_1\| \leq r_1, \qquad \|p_2 - c_2\| \leq r_2, \tag{2}$$

where $\|\cdot\|$ is the Euclidean norm. An example of the GDIP instance and its solution is depicted in Fig. 1.

Note that contrary to the DIP, the endpoints are not fixed in the GDIP, and they can be selected arbitrarily from the given regions, which significantly increases complexity of the problem. On the other hand, a solution of the GDIP enables to find a tight lower bound for a more general problem of the optimal Dubins path passing a sequence of regions, e.g., the DTRP.

A special version of the GDIP (further used to provide an optimal solution of the GDIP) is a degenerative case when the departure region P_1 is reduced to a single point p'_1. Such a problem is called the One-Sided GDIP (OS-GDIP).

Problem 3 (OS-GDIP)

$$\min_{\theta'_1,p'_2,\theta'_2} \mathcal{L}((p'_1,\theta'_1),(p'_2,\theta'_2)),$$
$$\text{s.t.} \quad \theta'_1 \in \Theta'_1,\ p'_2 \in P'_2,\ \theta'_2 \in \Theta'_2,$$

where all the variables are distinguished by a prime from Problem 2 to clarify the OS-GDIP is transformed from the GDIP. This notation is used in the following analysis.

4 Analysis of the GDIP

The GDIP is a continuous optimization problem minimizing the length of Dubins maneuver with respect to the given regions and intervals of the heading angles. The endpoints of the maneuver are selected from the compact regions which can be considered as an extension of the existing DIP. Thus, the optimization problem has six degrees of freedom as $\mathcal{L} : SE(2) \times SE(2) \to \mathbb{R}$. Two following ideas are utilized to reduce the complexity of the GDIP and provide its optimal solution.

First, the optimal solution of the GDIP is a path that is also the optimal solution of the corresponding DIP where the endpoints are fixed. This property is crucial because all the conditions for the optimal solution of the DIP summarized in Table 1 are directly applicable for the GDIP.

Secondly, the GDIP is reducible to the OS-GDIP, where one of the regions has zero radius, and thus the region is reduced to a single point. Such a transformation is possible because the GDIP is independent of the translation of its solution. The transformation is provided in the following paragraphs.

4.1 Transformation of the GDIP to the OS-GDIP and Vice-Versa

The main assumption for transforming an instance of the GDIP $\mathcal{G} = (P_1, \Theta_1, P_2, \Theta_2)$ to a transformed OS-GDIP instance $\mathcal{G}' = (p'_1, \Theta'_1, P'_2, \Theta'_2)$ is that any translation of the coordination system does not change the solution; the heading angles, the given intervals, and the maneuver length are all preserved. A solution of the original GDIP instance $\mathcal{G}$ is further denoted as $\tau = (p_1, \theta_1, p_2, \theta_2)$ and a solution of the transformed $\mathcal{G}'$ as $\tau' = (p'_1, \theta'_1, p'_2, \theta'_2)$. Therefore $\Theta_1 = \Theta'_1$, $\Theta_2 = \Theta'_2$ and also $\theta_1 = \theta'_1$, $\theta_2 = \theta'_2$, and thus we can focus only on the transformation of the endpoints and the regions.

To transform $\mathcal{G}$ into $\mathcal{G}'$, a solution of $\mathcal{G}$ is translated such that it starts at the origin, which reduces the dimensionality of the problem because the region P_1 is reduced to a single point $p'_1 = (0,0)$. The transformed region P'_1 contains only the origin and the region P'_2 can be determined using the dilation operation $\oplus$ from the mathematical morphology, which is also known as the Minkowski sum,

$$P'_1 = \{p'_1\} = \{(0,0)\}, \tag{3}$$
$$P'_2 = P_2 \oplus \check{P}_1 = \{p_b - p_a | p_a \in P_1, p_b \in P_2\}, \tag{4}$$

where $\check{P}_1$ is the reflection of P_1, i.e., $\check{P}_1 = \{-p | p \in P_1\}$. An example of the OS-GDIP is shown in Fig. 2.

Note the transformations (3) and (4) hold for regions of any shape as none of special properties are utilized. However, for the disk regions, the transformed P'_2 is also a disk with the radius r'_2 centered at c'_2

$$r'_2 = r_1 + r_2, \tag{5}$$
$$c'_2 = c_2 - c_1. \tag{6}$$

The **forward transformation** Φ_{12} of a feasible solution τ of the GDIP instance $\mathcal{G}$ to a feasible solution τ' of the OS-GDIP instance $\mathcal{G}'$ is a translation $\Phi_{12}(p) : p \to p'$ that moves the solution endpoint p_1 to $p'_1 = (0,0)$. The forward transformation is unique and it translates a point $p \in \mathbb{R}^2$ to the point $p' \in \mathbb{R}^2$ by $-p_1$

$$\Phi_{12}(p): \quad p \mapsto p - p_1. \tag{7}$$

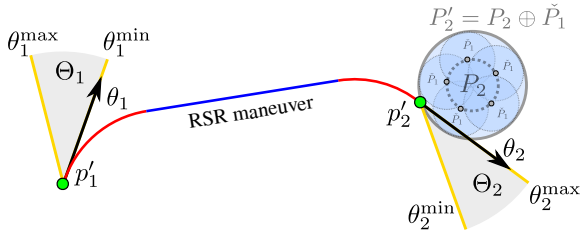

Fig. 2 OS-GDIP instance transformed from the GDIP instance in Fig. 1.

Lemma 1 *Any feasible solution τ of the particular GDIP instance $\mathcal{G}$ can be transformed by Φ_{12} (7) into a feasible solution τ' of the transformed OS-GDIP instance $\mathcal{G}'$ created from $\mathcal{G}$.*

Proof To prove the lemma, the endpoints of the transformed solution (Dubins maneuver) have to be in the given regions, i.e., $p_1' \in P_1'$ and $p_2' \in P_2'$. The first is always correct by the definition (3). The second endpoint is transformed to $p_2' = p_2 - p_1$ and using (6) it results into $(p_2' - c_2') = (p_2 - c_2) - (p_1 - c_1)$. Using inequalities (2) for the original GDIP instance $\mathcal{G}$, the terminal position p_2' is constrained by $\|p_2' - c_2'\| \leq r_2 + r_1$, and thus $p_2' \in P_2'$. □

The **backward transformation** Φ_{21} is not unique in general and for a feasible solution of the OS-GDIP instance $\mathcal{G}'$, there may exist multiple solutions of the original GDIP instance $\mathcal{G}$. This ambiguity is caused by different dimensionalities of $\mathcal{G}'$ and $\mathcal{G}$. In the original instance $\mathcal{G}$, two endpoints and two heading angles need to be determined, and thus the dimensionality of $\mathcal{G}$ is six; however, the departure point p_1' is fixed in $\mathcal{G}'$, and thus the dimensionality of $\mathcal{G}'$ is reduced to four. The backward transformation is unique only if p_2' is at the boundary of P_2'. Nevertheless, a universal formulation of the backward transformation $\Phi_{21}(p') : p' \to p$ exists as follows

$$\Phi_{21}(p'): \quad p' \mapsto p' + (c_1 - \lambda\,(p_2' - c_2'))\,, \tag{8}$$

where λ represents the ratio of the region radii in the original instance $\mathcal{G}$

$$\lambda = \frac{r_1}{r_1 + r_2}. \tag{9}$$

Lemma 2 *Any feasible solution τ' of the transformed OS-GDIP instance $\mathcal{G}'$ can be transformed by Φ_{21} (8) into a feasible solution τ of the original GDIP instance $\mathcal{G}$.*

Proof Analogously to the forward transformation, the back-transformed solution needs to fulfill the original constraints (2). The first endpoint can be transformed back by Φ_{21} as $p_1 = p_1' + c_1 - \lambda(p_2' - c_2')$, where p_1' can be omitted because $p_1' = (0, 0)$. Knowing $\|p_2' - c_2'\| \leq r_1 + r_2$ from (5) and by substituting it into the transformation Φ_{21} we get $\|p_1 - c_1\| \leq r_1$, and thus $p_1 \in P_1$. Similarly, for the second endpoint, $p_2 = p_2' + c_1 - \lambda(p_2' - c_2')$, and by subtracting $c_2 = c_2' + c_1$ (6) from both sides of the equation, it results in $p_2 - c_2 = (p_2' - c_2')(1 - \lambda)$. Using (5), as for the first endpoint, it proves $\|p_2 - c_2\| \leq r_2$, and thus $p_2 \in P_2$. □

Now, we need to show that the optimal solution of the transformed $\mathcal{G}'$ is the optimal solution of the original $\mathcal{G}$.

Lemma 3 *Let τ_*' be an optimal solution of the transformed OS-GDIP instance $\mathcal{G}'$, then, the solution τ transformed back by Φ_{21} (8) is an optimal solution of the original GDIP instance $\mathcal{G}$, i.e., τ is τ_*.*

Proof Let τ_* be an optimal solution of $\mathcal{G}$, then there exists an optimal solution τ_*' of $\mathcal{G}'$ with the same length because of Lemma 1. If τ_*' is transformed back by Φ_{21} (8) it has the same length of τ_* because of Lemma 2, and thus it is an optimal solution of $\mathcal{G}$. □

The main result of the forward (7) and backward (8) transformations is that any GDIP instance can be transformed to its one-sided version OS-GDIP. The transformation significantly reduces the search space of the original GDIP while all properties of the solution are preserved. Together with the DIP results Manyam et al. (2017), the OS-GDIP allows finding the optimal solution of the GDIP, which is proposed in the next section.

5 Optimal Solution of the GDIP

The main challenge of finding the optimal solution of a GDIP instance is related to the determination of the both departure and terminal configurations, i.e., (p_1, θ_1) and (p_2, θ_2), such that the length of the corresponding Dubins maneuver is minimized. The proposed solution is based on the transformation of the GDIP instance to the instance of the OS-GDIP using the transformations (3) and (4), which reduce the complexity of the problem as the first region P_1 of the GDIP becomes a single point p_2' in the OS-GDIP.

The OS-GDIP instance is solved using the necessary conditions for the optimal solution of the DIP summarized in Table 1, which clearly holds even for the GDIP and its sub-problem OS-GDIP. However, it is still necessary to address the selection of the second endpoint $p_2' \in P_2'$, which needs to be found optimally. Therefore, each possible maneuver type is addressed separately because their geometrical properties differ significantly. Thus, multiple candidate solutions are found

Table 2 All possibly optimal solutions of the GDIP

Case	Maneuver type	All possible maneuvers	Closed-form solution
1	S	S	YES
2	CS	L, R, LS, RS, SL, SR	YES
3	C_ψ	L_ψ, R_ψ	YES
4	CSC	LSL, RSR	YES
5	$CS\overline{C}$	LR, RL, LSR, RSL	YES
6	$C\overline{C}_\psi C$	LRL, RLR	YES
7	$C\overline{C}_\psi$	LR_ψ, RL_ψ, $L_\psi R$, $R_\psi L$	NO

from which the shortest one is selected similarly as for the DIP.

Finally, the optimal solution of the OS-GDIP instance is transformed to the solution of the original GDIP instance using the backward transformation (8). Since neither of the transformations changes the solution or its length, the proposed approach always finds the optimal solution. For the rest of this section, we provide a solution of the OS-GDIP instance.

5.1 Solving the OS-GDIP for Specific Types of Maneuvers

A solution of the GDIP follows the theoretical results of the DIP, and there exist 21 possibly optimal GDIP maneuvers that are all listed in Table 2. All maneuvers are categorized into seven basic types according to their geometrical properties. The original notation of the DIP is slightly modified and the arc segment is still denoted by C_ψ if the turning angle is greater than π, but $\overline{C}$ stands for an opposite turning direction. This modification enables to distinguish between CSC in which both arc segments have the same orientation and $CS\overline{C}$ for the opposite orientation, because the method of finding the optimal solution differs. For each type of the maneuvers, the optimal solution is provided separately.

The following notation is used in the rest of this section. The symbol $\mathcal{L}$ with a subscript defining the maneuver type denotes the optimal length of such Dubins maneuver. Particular segments of the same type in a single maneuver are distinguished by the subscript defining the order of the segment in the maneuver, e.g., C_1 is the first C segment of the CSC maneuver. An angle defined by two points p_i, c_j is denoted $\angle p_i c_j$, and analogously for three points.

5.1.1 S maneuver

The simplest maneuver contains a single straight segment S and its direction is given by the angle θ_S at the intersection Θ_S of the both given intervals

$$\theta_S \in \Theta_S, \quad \Theta_S = \Theta_1 \cap \Theta_2, \tag{10}$$

where Θ_S may contain up to two intervals. If the S maneuver is the optimal solution, one of the following cases occurs:

1.A If $p'_1 \in P'_2$ and $\Theta_S \neq \emptyset$ then $\mathcal{L}_S = 0$.
1.B If the above does not hold and $\angle p'_1 c'_2 \in \Theta_S$ then $\theta_S = \angle p'_1 s'_2$ and $\mathcal{L}_S = \|p'_1 - c'_2\| - r'_2$.

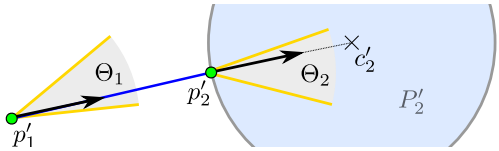

Fig. 3 An example of the straight maneuver solution of the OS-GDIP.

All of the cases can be found using basic algebra operations and an example of the 1.B case is shown in Fig. 3. Notice that S maneuvers for which $\mathcal{L}_S > 0$ and $\theta_S \neq \angle p'_1 s'_2$ cannot be optimal, even if θ_S is limited by the intervals Θ_1, Θ_2.

5.1.2 CS maneuvers

The next possible candidates for the optimal solution are the maneuvers of the CS type with a non-zero arc segment to differentiate it from the previous case. There are six possible combinations of maneuvers {R, L, LS, RS, SL, SR} of the CS type. But only the R and RS maneuvers are analyzed because L and LS maneuvers are analogous and SL and SR maneuvers are symmetric and can be addressed as follows. For the combinations SL and SR, an orientation of the solution is reverted and the original instance of the GDIP is transformed such that $r'_2 = 0$ and $r'_1 = r_1 + r_2$. Further, both Θ_1 and Θ_2 are reverted, and thus the problem is transformed to a different instance of the OS-GDIP where the solution is the LS or RS maneuver.

For the R and RS maneuvers, the departure angle $\theta_1 = \Theta_1^{\min}$ is known a priori. Thus, the center o_1 of the first arc segment is fixed and it remains to choose the terminal angle such that $\theta_2 \in \Theta_2$ and the length $\mathcal{L}_{RS}$ is minimized. Let the length of the circle segment be $\mathcal{L}_R > 0$ and $\mathcal{L}_S$ be the length of the straight segment. Then, three following cases can occur:

2.A The terminal angle is $\theta_2 = \Theta_2^{\max}$ and $\mathcal{L}_S = 0$.
2.B If $\|o_1 - c'_2\| \leq \rho$; the terminal point p'_2 is at the intersection between the arc segment and P'_2, and thus $\mathcal{L}_S = 0$.

2.C If $\|o_1 - c_2'\| > \rho$ then $\mathcal{L}_\mathrm{S} > 0$ and the extension of the straight segment passes through c_2'.

A closed-form solution exists for all three cases. The first two cases 2.A and 2.B are special boundary cases, which are obviously local optima; however, the optimality of the last case 2.C is proved in the following lemma.

Lemma 4 *If the optimal solution of the OS-GDIP instance is the RS maneuver and $\mathcal{L}_S > 0$, a line extension of the straight segment passes through c_2' (the center of P_2').*

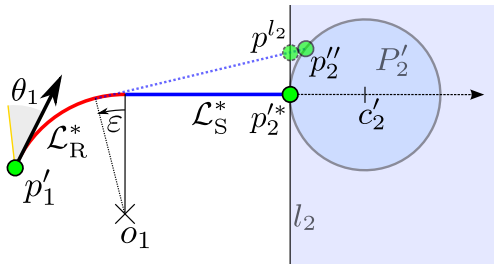

Fig. 4 RS maneuver of the CS type for various radii of P_2' depicted as the blue disks which become the blue half-plane in the limit case.

Proof Let $\mathcal{L}_\mathrm{R}^*$ and $\mathcal{L}_\mathrm{S}^*$ be lengths of the R and S segments of the RS maneuver for which Lemma 4 holds, and thus a line extension of the S segment passes through the center c_2' of the region P_2'. The end location of the maneuver is denoted as $p_2'^*$, see Fig. 4. To prove Lemma 4, we show that there exists no shorter RS maneuver by contradiction. Let assume there exist an alternative RS maneuver with the total length

$$\mathcal{L}_\mathrm{RS} < \mathcal{L}_\mathrm{R}^* + \mathcal{L}_\mathrm{S}^*, \tag{11}$$

which ends at $p_2'' \in P_2'$. Then, a line l_2 is defined such that it passes $p_2'^*$ and is perpendicular to the straight segment. The intersection of the alternative maneuver with l_2 is denoted as p^{l_2}, and the length of the first part of maneuver up to the point p^{l_2} is denoted as $\mathcal{L}_\mathrm{RS}^{l_2}$. If the assumption (11) holds, the first part of the alternate maneuver is also shorter, i.e., $\mathcal{L}_\mathrm{RS}^{l_2} < \mathcal{L}_\mathrm{R}^* + \mathcal{L}_\mathrm{S}^*$.

The total length $\mathcal{L}_\mathrm{RS}^{l_2}$ of the alternate maneuver ending at l_2 can be determined by

$$\mathcal{L}_\mathrm{RS}^{l_2} = \frac{\mathcal{L}_\mathrm{S}^* + \rho\,\sin(\varepsilon)}{\cos(\varepsilon)} + \mathcal{L}_\mathrm{R}^* - \rho\,\varepsilon, \tag{12}$$

where ε is the deviation from the direction towards c_2' (the center of P_2'). The derivative of the length function with respect to ε can be expressed as

$$\frac{\partial}{\partial\varepsilon}\mathcal{L}_\mathrm{RS}^{l_2} = \frac{\sin(\varepsilon)}{\cos^2(\varepsilon)}\,(\mathcal{L}_\mathrm{S}^* + \rho\,\sin(\varepsilon))\,. \tag{13}$$

The alternative RS maneuver can occur only if $\varepsilon \in (-\pi, \pi)$ and $\mathcal{L}_\mathrm{S}^* + \rho\,\sin(\varepsilon) > 0$; otherwise $\mathcal{L}_\mathrm{S} \not> 0$. An unique minimum occurs for $\varepsilon = 0$ for which $\mathcal{L}_\mathrm{RS}^{l_2} = \mathcal{L}_\mathrm{R}^* + \mathcal{L}_\mathrm{S}^*$. This is in the direct contradiction to (11), and thus there exist no shorter RS maneuver than the unique one for which Lemma 4 holds. □

5.1.3 C_ψ maneuvers

If p_1' and P_2' are close enough, maneuvers of the C_ψ type may become the optimal solution. The boundary cases of the heading angles are already covered by the CS type of the maneuvers, and therefore, such cases are forbidden for the C_ψ type of maneuvers, which can be expressed as

$$\theta_1 \in \Theta_1 \setminus \{\theta_1^{\min}, \theta_1^{\max}\}, \quad \theta_2 \in \Theta_2 \setminus \{\theta_2^{\min}, \theta_2^{\max}\}\,. \tag{14}$$

Lemma 5 *If the optimal solution of the OS-GDIP instance is of the C_ψ type, then $p_2' = \arg\max_{p \in P_2'} \|p - p_1'\|$.*

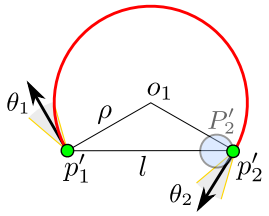

Fig. 5 R_ψ maneuver of the C_ψ type in the solution of the OS-GDIP.

Proof Let $\mathcal{L}_{\mathrm{C}_\psi}$ be the length of the C_ψ maneuver which depends on the distance $l = \|p_1' - p_2'\|$, see Fig. 5. Then

$$\mathcal{L}_{\mathrm{C}_\psi} = \rho\left(2\pi - 2\arcsin\left(\frac{l}{2\rho}\right)\right). \tag{15}$$

The length $\mathcal{L}_{\mathrm{C}_\psi}$ depends only on the distance l and it is independent on the specific p_2' location and its derivative can be expressed as

$$\frac{\partial}{\partial l}\mathcal{L}_{\mathrm{R}_\psi} = \frac{-2}{\sqrt{4 - \frac{l^2}{\rho^2}}}. \tag{16}$$

The derivative is always negative for the cases in which a maneuver of the C_ψ type can be constructed, i.e., for $l < 2\rho$. Thus, the terminal position p_2' of the optimal maneuver of the C_ψ type is such that the value of l is maximized. □

Notice the maneuver of the C_ψ type can be optimal only if the farthermost p_2' location meets $l < 2\rho$; otherwise there exists a shorter maneuver of a different type. Therefore, the necessary condition that a maneuver of the C_ψ type can be optimal is $\|p_1' - s_2'\| + r_2' < 2\rho$.

5.1.4 CSC maneuvers

Maneuvers of the CSC type contain two C segments C_1 and C_2 with the same orientation connected by the central S segment. All three segments are considered to have a non-zero length; otherwise the maneuver reduces into one of the above cases. Both the heading angles are known to be at the limits of the intervals based on the DIP conditions summarized in Table 1:

$$\text{CSC} \begin{cases} \text{LSL}: \theta_1 = \theta_1^{\max} \wedge \theta_2 = \theta_2^{\min}, \\ \text{RSR}: \theta_1 = \theta_1^{\min} \wedge \theta_2 = \theta_2^{\max}. \end{cases} \tag{17}$$

The total length of the C maneuvers ($\mathcal{L}_{C_1} + \mathcal{L}_{C_2}$) is given by θ_1, θ_2. However, the optimal position of p_2' needs to be found. Let p_2'' be a virtual endpoint of the maneuver of the CSC type, where the central S segment is omitted, see Fig. 6. Then, the following lemma can be formulated.

Lemma 6 *If the optimal solution of the OS-GDIP instance is a maneuver of the CSC type and all three segments have non-zero length, then* $p_2' = \arg\min_{p \in P_2'} \|p - p_2''\|$.

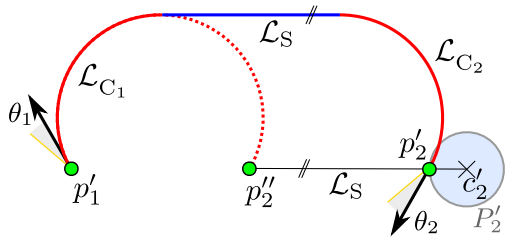

Fig. 6 RSR maneuver of the CSC type in the solution of the OS-GDIP.

Proof Since the sum of $\mathcal{L}_{C_1}$ and $\mathcal{L}_{C_2}$ is known a priori, the total length is influenced only by the length $\mathcal{L}_S$ of the straight segment. The orientation of the S segment is parallel to $p_2''p_2'$ and $\mathcal{L}_S = \|p_2'' - p_2'\|$. Therefore, $\mathcal{L}_S$ needs to be minimized to get the optimal solution. □

5.1.5 CS$\overline{\text{C}}$ maneuvers

Maneuvers of the CS$\overline{\text{C}}$ type contain two arc segments with the opposite orientations and the center S segment which may have zero length. Similarly to the previous case, the optimal heading angles are known a priori:

$$\text{CS}\overline{\text{C}} \begin{cases} \text{LSR}: \theta_1 = \theta_1^{\max} \wedge \theta_2 = \theta_2^{\max}, \\ \text{RSL}: \theta_1 = \theta_1^{\min} \wedge \theta_2 = \theta_2^{\min}. \end{cases} \tag{18}$$

In contrast to the previous CSC type, this type of maneuvers is more complex because the lengths of the arc segments cannot be determined directly from θ_1, θ_2. Therefore, a transformation to a different OS-GDIP instance is considered.

Lemma 7 *If the optimal solution of the OS-GDIP is a maneuver of the CS$\overline{\text{C}}$ type, the problem instance can be transformed into an OS-GDIP instance where the solution is of the CS type.*

Proof Since θ_1, θ_2 are fixed, the center o_1 of the first C segment is given by the location of p_1' and θ_1. The second center o_2 lies inside the disk region O_2 of its possible locations. The region O_2 is determined based on P_2' which is translated by the vector $\mathbf{g}_2$ perpendicular to θ_2 and with the magnitude of ρ. Orientation of $\mathbf{g}_2$ depends on the direction of the last turn:

$$\mathbf{g}_2 = \begin{cases} \rho\,(-\sin\theta_2, \cos\theta_2) & \text{for } \_\_\text{L maneuvers}, \\ \rho\,(\sin\theta_2, -\cos\theta_2) & \text{for } \_\_\text{R maneuvers}. \end{cases} \tag{19}$$

where $\_$ stands for an arbitrary path segment. Then, the region O_2 is defined as follows (see Fig. 7):

$$O_2 = \{p_2' + \mathbf{g}_2 \mid p_2' \in P_2'\}. \tag{20}$$

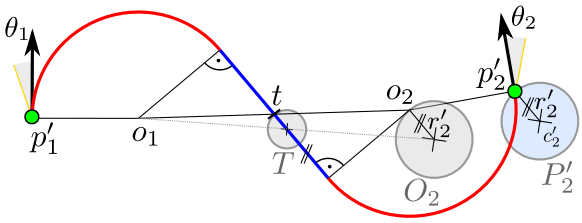

Fig. 7 RSL maneuver of the CS$\overline{\text{C}}$ type in the solution of the OS-GDIP.

An important point of the CS$\overline{\text{C}}$ maneuver is the center t of the segment S because it is also the origin of the point of symmetry for the whole maneuver. Thus, the origin t is a midpoint between the centers c_1 and c_2. The set T of all possible t locations can be determined based on o_1 and O_2:

$$T = \left\{ \frac{o_1 + o_2}{2} \mid o_2 \in O_2 \right\}. \tag{21}$$

The main idea is that the whole maneuver can be easily constructed once the origin t is known. Thus, the problem of finding the shortest CS$\overline{\text{C}}$ maneuver can be transformed to the problem of finding the optimal location of t.

Since t is an origin of the center symmetry, it splits the maneuver to two parts. One of the parts may be longer to compensate the difference between departure and terminal heading angles $|\theta_1 - \theta_2|$. The difference is

constant and not influenced by the selection of t, and thus the length of the second part is directly proportional to the first one.

Since the lengths of both parts of the maneuver divided by t are proportional, it is sufficient to optimize only the length of the first part to find the optimal solution. Thus, the problem is transformed to find the shortest CS maneuver from p'_1 to the region T. The transformed problem is an GDIP instance G_{CS} for which the departure point and heading angle are fixed, the arrival point lies in T, and the corresponding heading angle is arbitrary, i.e., $G_{\mathrm{CS}} = (\, p'_1, \theta_1, T, [0, 2\pi)\,)$. □

As a result of Lemma 7, the problem of finding a maneuver of the CS$\overline{\mathrm{C}}$ type is transformed into a relatively easy problem for which a closed-form solution exists as it is shown in Section 5.1.2.

5.1.6 C$\overline{\mathrm{C}}_{\psi}$C maneuvers

If $\|p'_1 - p'_2\| < 4\rho$, the maneuvers of the C$\overline{\mathrm{C}}_{\psi}$C type can be the optimal solution because one of the maneuvers of the CS$\overline{\mathrm{C}}$ type cannot be constructed. The optimal heading angles are known a priori

$$\mathrm{C}\overline{\mathrm{C}}_{\psi}\mathrm{C} \begin{cases} \mathrm{LR}_{\psi}\mathrm{L} : \ \theta_1 = \theta_1^{\max} \ \wedge \ \theta_2 = \theta_2^{\min}, \\ \mathrm{RL}_{\psi}\mathrm{R} : \ \theta_1 = \theta_1^{\min} \ \wedge \ \theta_2 = \theta_2^{\max}. \end{cases} \tag{22}$$

Similarly to the CS$\overline{\mathrm{C}}$ type of maneuvers, the center o_1 of the first C segment is known and the third center o_3 lies inside the disk region O_3 derived from P'_2, see Fig. 8. Then, the third center o_3 is determined based on the following lemma.

Lemma 8 *If the optimal solution of the OS-GDIP is a maneuver of the C$\overline{\mathrm{C}}_{\psi}$C type, then* $o_3 = \arg\max_{s \in O_3} \|s - o_1\|$.

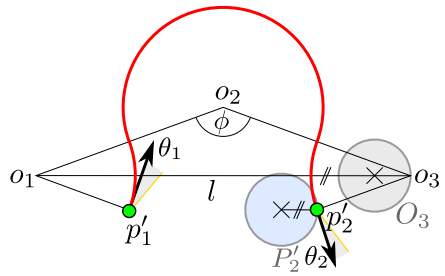

Fig. 8 LRL maneuver of the C$\overline{\mathrm{C}}_{\psi}$C type in the solution of the OS-GDIP.

Proof The length of the maneuver can be determined based on the angle $\phi = \angle o_1 o_2 o_3$

$$\mathcal{L}_{\mathrm{C}\overline{\mathrm{C}}_{\psi}\mathrm{C}} = \rho\,(\,|\theta_1 - \theta_2| + 2k\pi - 2\phi)\,, \tag{23}$$

where $k \in \mathbb{Z}$ is for the angle normalization. Since θ_1, θ_2, and k are fixed for the specific maneuver type, the only remaining variable in (23) is the angle ϕ which needs to be maximized to get the shortest solution. Thus, the distance $l = \|o_1 - o_3\|$ needs to be maximized because $\frac{\partial \phi}{\partial l} > 0$ for $0 < l < 4\rho$. □

Notice o_3 can be found by a closed-form expression because O_3 is a circular region. Having o_1 and o_3, the maneuver is well defined and easy to construct. A necessary condition for C$\overline{\mathrm{C}}_{\psi}$C to be optimum is

$$\forall o_3 \in O_3 : \|o_1 - o_3\| < 4\rho. \tag{24}$$

Otherwise, it would be possible to construct a shorter CS$\overline{\mathrm{C}}$ maneuver.

5.1.7 C$\overline{\mathrm{C}}_{\psi}$ maneuvers

The last type of maneuvers is C$\overline{\mathrm{C}}_{\psi}$ which can also occurs only if $\|p'_1 - p'_2\| < 4\rho$. There may exist up to four maneuvers for which one of the heading angles is known:

$$\mathrm{C}\overline{\mathrm{C}}_{\psi} \begin{cases} \mathrm{L}\overline{\mathrm{R}}_{\psi} : \ \theta_1 = \theta_1^{\max} \ \wedge \ \theta_2 \in \Theta_2, \\ \mathrm{R}\overline{\mathrm{L}}_{\psi} : \ \theta_1 = \theta_1^{\min} \ \wedge \ \theta_2 \in \Theta_2, \\ \overline{\mathrm{R}}_{\psi}\mathrm{L} : \ \theta_1 \in \Theta_1 \ \wedge \ \theta_2 = \theta_2^{\min}, \\ \overline{\mathrm{L}}_{\psi}\mathrm{R} : \ \theta_1 \in \Theta_1 \ \wedge \ \theta_2 = \theta_2^{\max}. \end{cases} \tag{25}$$

Only the maneuver L$\overline{\mathrm{R}}_{\psi}$ of the C$\overline{\mathrm{C}}_{\psi}$ type is further studied because other maneuvers share the same properties. Let o_1 and o_2 be the centers of the C segments, then the length of the maneuver depends on p'_2:

$$\mathcal{L}_{\mathrm{L}\overline{\mathrm{R}}_{\psi}} = \rho(2\pi - \alpha + \beta + \varphi), \tag{26}$$

where $\varphi = \angle p'_1 o_1 p'_2$ and $\alpha = \angle o_1 o_2 p'_2$, $\beta = \angle p'_2 o_1 o_2$ which depends on the distance $d = \|o_1 - p'_2\|$, see Fig. 9. The maneuver length from (26) can be expressed in the

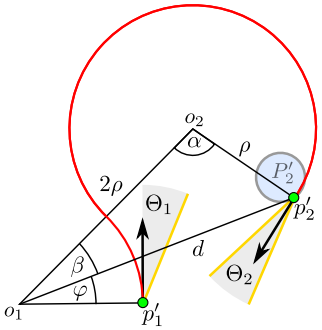

Fig. 9 L$\overline{\mathrm{R}}_{\psi}$ maneuver of the C$\overline{\mathrm{C}}_{\psi}$ type in the solution of the OS-GDIP.

polar coordination system of (φ, d) as

$$\mathcal{L}_{\mathrm{L}\overline{\mathrm{R}}_\psi} = \rho \left[2\pi - \cos^{-1}\left(\frac{5\rho^2 - d^2}{4\,\rho^2}\right) + \cos^{-1}\left(\frac{3\rho^2 + d^2}{4\,d\,\rho}\right) + \varphi \right]. \quad (27)$$

The derivatives of the maneuver length are

$$\frac{\partial}{\partial\varphi}\mathcal{L}_{\mathrm{L}\overline{\mathrm{R}}_\psi} = \rho, \quad \frac{\partial}{\partial d}\mathcal{L}_{\mathrm{L}\overline{\mathrm{R}}_\psi} = \frac{3\rho^2 - 3d^2}{d\sqrt{-d^4 + 10d^2\rho^2 - 9\rho^4}}. \quad (28)$$

From the domain of the second derivative according to d, the necessary condition for the $\mathrm{C}\overline{\mathrm{C}}_\psi$ maneuver to exist is

$$\rho \leq d \leq 3\rho, \quad (29)$$

which corresponds to a direct geometrical representation. Thus, the signs of both derivatives are fixed

$$\frac{\partial}{\partial\varphi}\mathcal{L}_{\mathrm{L}\overline{\mathrm{R}}_\psi} > 0, \quad \frac{\partial}{\partial d}\mathcal{L}_{\mathrm{L}\overline{\mathrm{R}}_\psi} < 0. \quad (30)$$

Based on these preliminaries, the optimality of the maneuver is shown in Lemma 9.

Lemma 9 *If the optimal solution of the OS-GDIP instance is the $C\overline{C}_\psi$ maneuver, the terminal position p'_2 lies at the boundary of the departure region P'_2.*

Proof The signs of both length derivatives are fixed, and thus the minimum of the length function is at the boundary of P'_2 or a maneuver of the $\mathrm{C}\overline{\mathrm{C}}_\psi$ type is not optimal. □

Notice the second derivative of $\mathcal{L}_{\mathrm{L}\overline{\mathrm{R}}_\psi}$ over d can be expressed as

$$\frac{\partial^2}{\partial d}\mathcal{L}_{\mathrm{L}\overline{\mathrm{R}}_\psi} = \frac{3(9\rho^4 - 2\rho^2 d^2 + d^4)}{d^2(d^2 - 9\rho^2)\sqrt{-9\rho^4 + 10\rho^2 d^2 - d^4}}, \quad (31)$$

for which $\frac{\partial^2}{\partial d}\mathcal{L}_{\mathrm{L}\overline{\mathrm{R}}_\psi} < 0$ holds if d is in the interval from (29). The second derivative over φ is always zero, i.e., $\frac{\partial^2}{\partial\varphi}\mathcal{L}_{\mathrm{L}\overline{\mathrm{R}}_\psi} = 0$.

Knowing one of the second derivatives is zero and the other derivative is always negative, the problem can be seen as an optimization problem which contains an unique minimum. Furthermore, the position of p'_2 in the optimal solution is known to be at the boundary of P'_2, which reduces the problem to a convex optimization problem with a single variable. A closed-form formula is not known but the problem can be easily solved by a numerical method, such as hill-climbing.

6 Proposed Tight Lower Bound and Upper Bound Solutions of the DTRP

The introduced GDIP is motivated to find the optimal solution of the Dubins TSP with Neighborhoods (DTSPN). Even though this ultimate goal is still open, we demonstrate the importance of the optimal solution of the GDIP for solving Dubins routing problems through a set of regions in a solution of the DTSPN for which the sequence of visits to the regions is given. We explicitly call the problem as the Dubins Touring Regions Problem (DTRP) to distinguish it from the DTSPN which also includes the sequencing part of the underlining TSP. Therefore, we formally define the DTRP in Section 6.1, and in Section 6.2, we propose a tight lower bound procedure for the DTRP using the optimal solution of the introduced GDIP. Finally, the proposed informed sampling-based procedure to iteratively refine the lower bound and find a high-quality solution of the DTRP is presented in Section 6.3.

6.1 Dubins Touring Regions Problem (DTRP)

The **Dubins Touring Regions Problem** (DTRP) denotes the problem to find the shortest curvature-constrained path through a given sequence of regions. For n compact regions $\mathcal{R} = \{R_1, \ldots, R_n\}$, $R_i \subset \mathbb{R}^2$, the requested multi-goal path can be defined by a sequence of configurations $\mathcal{Q} = (q_1, \ldots, q_n)$. Then, the DTRP can be defined as an optimization Problem 4.

Problem 4 (DTRP)

$$\begin{aligned} \text{minimize}_{\,\mathcal{Q}} \quad & \mathcal{L}(q_n, q_1) + \sum_{i=1}^{n-1} \mathcal{L}(q_i, q_{i+1}) \\ \text{s.t.} \quad & \\ & \mathcal{Q} = (q_1, \ldots, q_n) \\ & q_i = (x_i, y_i, \theta_i),\ i = 1, \ldots, n \text{ for} \\ & (x_i, y_i) \in R_i \text{ and } \theta_i \in \mathbb{S}^1, R_i \in \mathcal{R}, R_i \subset \mathbb{R}^2, \end{aligned}$$

where $\mathcal{L}(q_i, q_{i+1})$ is the Dubins distance between two consecutive visiting configurations q_i and q_{i+1}.

The idea of the introduced DTRP is to separate the sequencing part of the DTSPN from the continuous optimization and focus on the continuous optimization.

We can leverage on the existing sampling-based approaches to the DTP and we can address the DTRP by sampling of the regions and heading intervals into a discrete set of the interval samples. The introduced GDIP can be then employed in solving the instances defined by the sampled intervals, and we can establish a tight lower bound of the DTRP.

6.2 Tight Lower Bound for the DTRP

Both the optimal heading angle and the optimal location within the region need to be determined simultaneously for each visiting configuration of the DTRP which makes this optimization problem challenging.

The proposed tight lower bound follows the idea of Manyam et al. (2017) on the tight lower bound for the DTP, i.e., the problem of finding the shortest Dubins path through a sequence of the given locations. The idea is that the possible heading angles are split into a discrete set of angle intervals, and the lower bound is computed as the shortest tour based on the solution of the DIP connecting the angle intervals by the shortest Dubins path. Note the lower bound is not a feasible solution of the DTP because it contains discontinuities in the heading angle. The idea of the DTP lower bound is extended to the DTRP where a particular location of the visiting configuration can arbitrarily be selected within the corresponding region. Therefore, the original DIP formulations cannot be utilized, and the introduced GDIP is necessary to address the lower bound of the DTRP.

We follow the idea to split the possible values of the heading angle into a discrete set of intervals with the heading resolution ω_H. Thus, the size of the heading interval Θ is $\|\Theta\| = \frac{2\pi}{\omega_H}$, which also represents the maximum discontinuity in the heading of the lower bound solution. In addition to the heading intervals, the possible location of the visiting configuration needs to be sampled similarly. The regions are two-dimensional sets, but we consider the particular visiting configuration is at the boundary of the region because any feasible solution intersects the boundary of the region. Let a disk-shaped target region R_i with the radius δ be centered at c_i; then, the visiting configuration can be encoded by a single angle value γ as

$$(x_i, y_i) = c_i + \delta(\cos\gamma, \sin\gamma). \tag{32}$$

All possible locations can be then divided into a discrete set of neighborhoods defined by the intervals Γ which represent arcs on the boundary of the particular region to be visited. Let the position resolution be ω_P and Γ is an angle interval of γ; then, the size of the interval is $\|\Gamma\| = \frac{2\pi}{\omega_P}$. An example of the sampled intervals of the possible location of the visiting configuration at the border of the region is depicted in Fig. 10.

Each sampled arc segment is bounded by a disk-shaped region defined by the circumscribed circle to directly utilize the found optimal solution of the GDIP. The center c of the region is in the middle between two endpoints of the specific circular arc and its radius

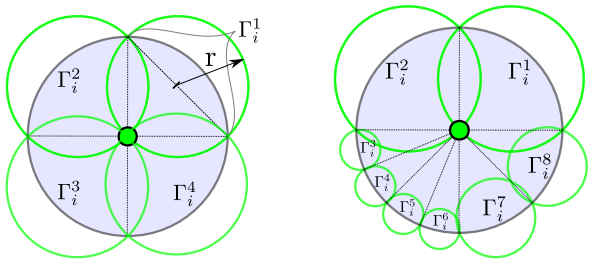

(a) Uniform sampling, position resolution $\omega_P = 4$.

(b) Irregular sampling, position resolution $\omega_P \in [4, 16]$.

Fig. 10 An example of location sampling of the original disk-shaped region shown in the light blue into a set of position intervals (green) as the arcs on the region boundary defined by the angle intervals Γ_i^j for the region R_i.

r equals half of the distance between these two endpoints. The radius r of the circumscribed region can be expressed as

$$r = \begin{cases} \delta \sin\left(\frac{\pi}{\omega_P}\right) & \text{if } \omega_P \geq 2 \\ \delta & \text{otherwise} \end{cases}, \tag{33}$$

where δ is the radius of the original disk-shaped region. Notice the radius r goes to zero for increasing resolution ω_P (i.e., increasing number of the samples)

$$\lim_{\omega_P \to \infty} r(\omega_P) = \lim_{\omega_P \to \infty} \delta \sin\left(\frac{\pi}{\omega_P}\right) = 0. \tag{34}$$

Based on the idea of sampling the continuous variables into finite set of intervals, the space of all possible visiting configurations for the target region R_i is divided into a discrete set of k_i samples $S_i = \{s_i^1, \ldots, s_i^{k_i}\}$. Each sample $s_i^j = (\Gamma_i^j, \Theta_i^j)$ is defined by the circumscribed region of the corresponding position interval Γ_i^j and heading interval Θ_i^j. The size of the intervals Γ_i^j and Θ_i^j is given by the specific position resolution ω_P and heading resolution ω_H, respectively.

The sampling $\mathcal{S} = \{S_1, \ldots, S_n\}$ of the DTRP is constituted of all sampled intervals for the specific target regions. Based on $\mathcal{S}$, lower bound paths can be computed as the optimal solution of the GDIP for each pair of the consecutive samples corresponding to the consecutive regions in the given sequence. The individual lower bound for the path between two sampled intervals of two consecutive regions can be connected into a global search graph that is depicted in Fig. 11.

Then, the lower bound of the DTRP can be determined using the constructed graph structure and finding the shortest tour over the partial lower bound paths determined as the individual solutions of the GDIP for the particular sampled intervals corresponding to the

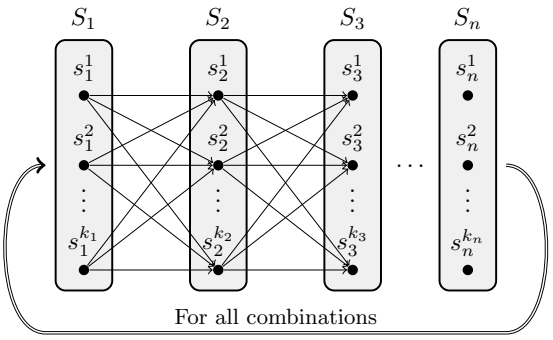

Fig. 11 A graph-based structure that represents the sampled intervals of the regions in the sequence. Finding the shortest path in the graph corresponds to the lower bound estimation of the length of the shortest Dubins multi-goal trajectory through the given sequence of regions.

consecutive regions. Notice the determined tour representing the lower bound is not a feasible solution of the DTRP because it contains discontinuities in the position and heading of the particular sampled configurations of two consecutive regions; moreover, the lower bound solution is not even guaranteed to intersect the given regions as a result of the proposed position sampling. The size of the discontinuities is limited by the utilized resolutions ω_P and ω_H and the lower bound is assumed to converge to the optimal solution if the resolutions go to infinity.

The most straightforward way how to split possible position and heading intervals of the visiting configurations is to utilize uniform sampling for creation of the set of the sampled intervals $\mathcal{S}$. Unfortunately, the number of samples quickly grows with the increasing resolutions ω_P and ω_H and finding the shortest path in the corresponding search graph is computationally demanding. We can establish bounds on the computational complexity for the uniform sampling as follows.

Let $\omega_{\max}$ be the maximal resolution and $\omega_P = \omega_H = \omega_{\max}$ for the uniform sampling. Then each of n regions in the sequence is sampled by $k = \omega_{\max}^2$ samples and the number of needed evaluations of the GDIP between each pair of the samples corresponding to two consecutive regions can be bounded by $\mathcal{O}(nk^2)$ or $\mathcal{O}(n\omega_{\max}^4)$ in the term of the maximal resolution. Consecutively, the final lower bound is computed as the shortest tour in the search graph depicted in Fig. 11. The complexity of finding the tour can be bounded by $\mathcal{O}(nk^3)$ if a dynamic programming approach is utilized. Thus, a determination of the lower bound of the DTRP instance with the n regions and uniform sampling with the resolution $\omega_{\max}$ can be bounded by $\mathcal{O}(n\omega_{\max}^6)$.

6.3 Informed Sampling-based Approach to the DTRP

The proposed solution to the DTRP is based on determining a tight lower bound of the DTRP by iterative increasing the resolution ω of the sampled intervals. Although the uniform sampling can be eventually utilized, it is found to be computationally demanding, and therefore, we follow the idea of the informed sampling presented in (Faigl et al., 2017) for solution of the DTP. The idea of the informed sampling is to refine (split) the sampling $\mathcal{S}$ in the most promising sampled intervals that will tighten the lower bound, i.e., increase the value of the computed lower bound. It is proceeded by refining the sampled intervals that are part of the currently determined the shortest lower bound tour.

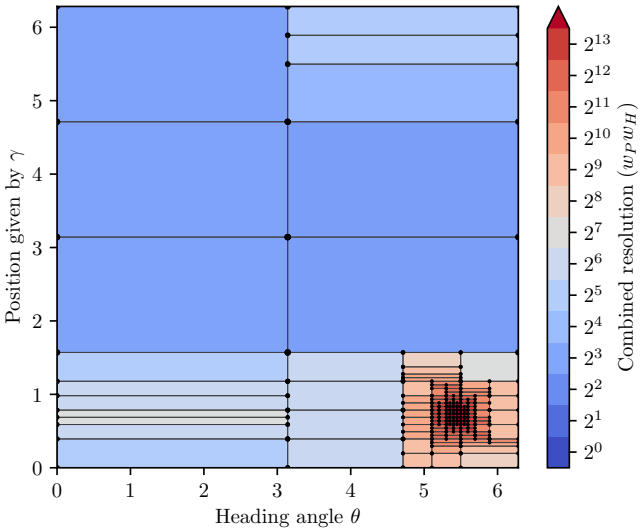

Fig. 12 An example of the informed sampling for the left bottom region of the DTRP instance shown in Fig. 13.

Each refinement removes the selected sample that is replaced by its two refined intervals. Although the refinement of the position and angle intervals can be alternated, the position refinement is prioritized because a faster convergence has been observed in random instances of the DTRP with $\delta = 1$; however, angle intervals refinement may be more beneficial for $\delta \ll 1$. Therefore, the refinement is performed for the position interval if the position resolution is lower than the current desired resolution ω. Here, it is worth noting that the position and heading resolutions can differ significantly for each partial sample not only because of prioritized position intervals but also as a result of the iterative refinement and convergence to the tight lower bound estimation. An example of the interval distribution is shown in Fig. 12.

The key idea of the informed sampling is to find the same lower bound value as for the uniform sampling but using a much smaller number of the samples. The convergence to the same results can be expressed in the following lemma.

Lemma 10 *Informed sampling provides the same lower bound for the DTRP as the uniform sampling if the position and heading resolutions in the final tour are the same as for the uniform sampling.*

Proof The lower bound is computed as the shortest tour in the graph that is created using the optimal solution of the corresponding instances of the GDIP. If a specific sample is divided into two samples (either by splitting position or heading interval), the optimal solution of the corresponding instances of the GDIP cannot decrease. As a result, the lower bound for a lower resolution cannot be greater than the lower bound for a denser resolution. Therefore, if the lower bound for the uniform and informed sampling differs then; the tour found for the informed sampling contains samples with a lower resolution which is in a contradiction with the assumption, and a further refinement should be applied. □

Even though the lower bound is an important contribution to the solution of the DTRP, the bound itself does not provide a feasible solution of the DTRP. However, the proposed informed sampling is expected to sample the space around the optimal solution densely, and the distribution of the informed sampling includes information about the optimal solutions. Hence, we propose to utilize the samples $\mathcal{S}$ generated by the informed sampling for determining a high-quality solution of the DTRP. The only modification is that instead of constructing the search graph (shown in Fig. 11) using the optimal solution of the GDIP, the corresponding Dubins maneuvers to the feasible configurations are utilized. In particular, the feasible configuration is selected based on the specific sample $s = (\Gamma, \Theta)$ such that the position is determined by (32) where the angle $\gamma = \min(\Gamma)$ and the heading angle $\theta = \min(\Theta)$. Thus, the feasible configurations correspond to the corners of the sampled intervals depicted as small black disks in Fig. 12. Notice, the computational complexity of finding the shortest tour remains the same as for the lower bound because the number of samples/configurations remains the same, and thus a feasible solution of the DTRP is determined in a similar way.

Both approaches for finding a lower bound and a feasible solution of the DTRP based on the informed sampling can be combined in a single iterative procedure that is summarized in Algorithm 1. The main benefit of the combined method is that it enables to compute the relative gap between the lower bound and the found solution at every iteration of the refinement. Thus the procedure has any-time property and the gap is improving with increasing resolution ω. The proposed iterative algorithm proceeds as follows.

Algorithm 1: Informed sampling-based solution of the DTRP using optimal solution the GDIP.

Input: $\mathcal{R}$ – Sequence of the regions to be visited
Input: $\omega_{\max}$ – Maximal requested resolution
Output: $\mathcal{Q}$ – Visiting configurations of the final tour
Output: $\mathcal{L}_L$ – Lower bound (unfeasible)
Output: $\mathcal{L}_U$ – Upper bound (feasible)

```
ω ← 1                          // initial resolution
S ← sampleIntervals(R)         // initial intervals
L_L ← 0                        // init lower bound
L_U ← ∞                        // init upper bound
while ω ≤ ω_max do
    (S, L_L) ← refineLowerBound(R, ω, S)
    (Q, L_U) ← findFeasibleSolution(R, S)
    ω ← 2 ω
end
return Q, L_L, L_U
```

The procedure starts with the lowest possible resolution $\omega = 1$ and the samples are gradually refined to meet the maximal requested resolution $\omega_{\max}$. The initial samples, created by the procedure *sampleIntervals*, consist of the original regions R_i corresponding to the position interval $\Gamma_i^1 = [0, 2\pi)$ and the full heading angle interval $\Theta_i^1 = [0, 2\pi)$. Then, the algorithm continues with the main loop in which the *refineLowerBound* procedure finds the shortest lower bound tour and refine the selected samples if their resolution is lower than the current resolution ω. After that, a feasible path is found for the current sampling sets $\mathcal{S}$ in the procedure *findFeasibleSolution*. Thus, both the lower and upper (feasible solution) bounds are updated in each iteration of the algorithm, and the optimality gap is determined. Notice the gap cannot increase for the refined sampling and it is decreased for most of the cases.

Regarding the particular implementation of the algorithm, the optimal solutions of the GDIP for determining the lower bound and Dubins maneuvers for the feasible solution are not computed in each iteration. Instead, the computed values are stored and utilized in the next iterations if the specific intervals are not refined to improve real computational requirements of the algorithm. The results on the computational requirements are reported in the following section.

7 Evaluation Results

The proposed optimal solution of the introduced GDIP and its practical deployment in the solution of the DTRP

have been empirically verified in two evaluation scenarios. In the first scenario, we evaluate the real computational requirements of the optimal solution of the GDIP for the overall solution, but also for each possible case separately to study the optimal solution in more detail. In the second scenario, the convergence of the proposed algorithm for the DTRP based on the GDIP is demonstrated for problems with the increasing number of the target regions.

The optimal solution of the GDIP and solution of the DTRP have been implemented[2] in C++ and compiled by the Clang ver. 6.0.0 with the enabled optimizations -O3. All the reported results have been computed using a single core of the Intel Core i5-7600K CPU running at 3.8 GHz.

7.1 Real Computational Requirements of the GDIP

The optimal solution of the GDIP can be computed very efficiently because almost all the cases can be found by a closed-form expression. The only remaining case ($C\overline{C}_\psi$) is transformable to a convex optimization with a single variable and thus solved quickly. However, the number of possible maneuvers is higher than in a solution of the simple point-to-point Dubins maneuver, and therefore, the average computational time of finding the optimal solution has been measured for three different problems: Dubins maneuver, DIP, and the proposed GDIP. For each problem, 10^6 random instances have been generated with the same generation setting: the minimum turning radius $\rho = 1$ and the points p_1, p_2 are uniformly selected from the box $p_1, p_2 \in [0, 10] \times [0, 10]$. The headings angles are uniformly selected as $\theta_1, \theta_2 \in [0, 2\pi]$ for the Dubins maneuver problem and the boundaries of the angle intervals are arbitrarily selected $\theta_1^{\min}, \theta_1^{\max}, \theta_2^{\min}, \theta_2^{\max} \in [0, 2\pi]$ for the DIP. Finally, the GDIP instances are further specified by the centers c_1 and c_2 of the regions P_1 and P_2, respectively, that are the same as the points p_1 and p_2, and the radii of the regions are uniformly selected as $r_1, r_2 \in [0, 1]$.

Table 3 Average computational time per one solution

Problem	Max. #	Time [μs]	Time ratio
Dubins maneuver	6	0.374	1.0
DIP	23	1.114	3.0
GDIP	26	5.417	14.5

The average computational times are reported in Table 3. The results show that the computation of a single Dubins maneuver takes less than 0.4 μs while the number of examined maneuvers (Max. #) is only six. Finding the optimal solution for the DIP is about three times more computationally demanding because 23 maneuvers are examined in the total. Notice this number of examined maneuvers is greater then 21 distinguishable maneuvers in Table 1 because of implementation details where some maneuvers need to be examined in more specific cases. The proposed optimal solution for the GDIP needs to compute only three more maneuvers. However, a computation of the individual cases are slightly more complex for the GDIP, and thus a computation of a single optimal solution is about 15 times more demanding than computing the optimal Dubins maneuver.

The proposed optimal solution of the GDIP is based on seven cases, each with specific maneuver type, and a number of possible maneuvers, see Table 2. The solution is computed such that each maneuver type is constructed separately and the shortest path is selected at the end. Therefore, we can further study specific cases and analyze how many times each particular maneuver is the optimal solution. The above results can be thus divided according to the specific cases, and the results are provided in Table 4, where the notation of the maneuver types from Section 4 is followed to distinguish all possible cases clearly. In addition to the maximum number of the determined maneuvers (denoted Max. #), the average number of successfully constructed maneuvers (denoted Avg. #), i.e., the maneuvers that can be constructed, the average number of maneuvers which are the optimal solution (denoted Opt. #), and the average computational time are reported. The results show that a feasible solution exists for any GDIP instance because CSC type can always be constructed, but it likely not to be the optimum. In contrast, if the S maneuver is successfully constructed no other maneuver can be shorter. Notice that more than six maneuvers are constructed to find a single optimal solution on the average.

7.2 Evaluation of the Proposed Solution to the DTRP

The proposed solution to the DTRP using its tight lower bound based on the optimal solution of the GDIP has been evaluated for a set of randomly generated DTRP instances[3] with $n \in \{10, 20, 50, 70, 100\}$, $\delta = 1$, and $\rho = 1$. The sequence of visits to the regions has

[2] Source codes are available at `https://github.com/comrob/gdip`.

[3] The instances have been generated with the relative density $d = 0.3$ and possibly overlapping regions where the region centers are randomly placed with the squared bounding box with the size $s = \rho\sqrt{n}/d$.

Table 4 Statistics of maneuver types in the optimal solution of the GDIP computed by the provided reference implementation

Case	Type	Maneuvers	Max. #	Avg. #	Opt. #	$\frac{\text{Avg.}}{\text{Max.}}$ [%]	$\frac{\text{Opt.}}{\text{Avg.}}$ [%]	$\frac{\text{Opt.}}{\text{Max.}}$ [%]	Time [μs]
1.A	S	S	1	0.0272	0.0272	2.72	100.00	2.72	0.03
1.B	S	S	1	0.2426	0.2426	24.26	100.00	24.26	0.04
2.A	C(S)	L, R	4*	0.1189	0.0146	2.97	12.32	0.37	0.58
2.B	C(S)	L, R	4*	0.2002	0.0317	5.00	15.86	0.79	0.47
2.C	CS	LS, RS, SL, SR	4	1.9498	0.4531	48.75	23.24	11.33	0.81
3	C_ψ	L_ψ, R_ψ	2	0.0026	0.0022	0.13	86.30	0.11	0.02
4	CSC	LSL, RSR	2	2.0000	0.1067	100.00	5.34	5.34	0.43
5	$CS\overline{C}$	LR, RL, LSR, RSL	2†	1.9406	0.1186	97.03	6.11	5.93	1.71
6	$C\overline{C}_\psi C$	LRL, RLR	2	0.1124	0.0009	5.62	0.84	0.05	0.08
7	$C\overline{C}_\psi$	LR_ψ, RL_ψ, $L_\psi R$, $R_\psi L$	4	0.0335	0.0022	0.84	6.60	0.06	0.91
Total			26	6.6278	1.0000	25.49	15.09	3.85	5.10

*Maneuvers need to be examined from both sides, and thus the number is twice the number of maneuvers.
†LR and LSR maneuver are examined in a single step and the same for RL and RSL, respectively.

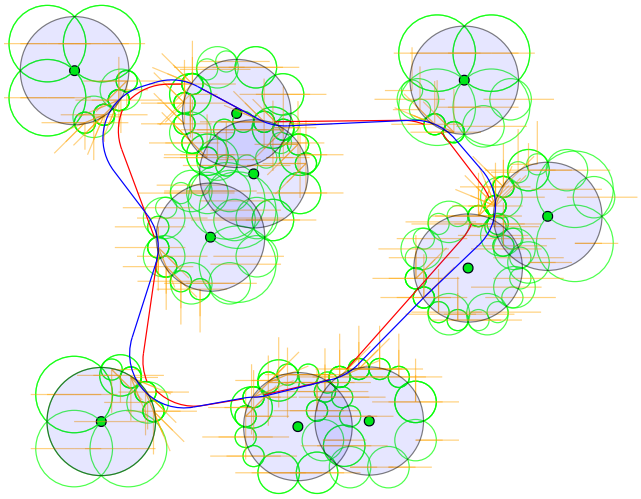

Fig. 13 An example of the DTRP instance with $n = 10$ target regions each with the radius $\delta = 1$ (visualized as the light blue disks) and $\rho = 1$. The lower bound path is 17.68 long (red) and a feasible solution is 22.07 long (blue) both determined in 0.66 s for $\omega_{\max} = 16$. The green circles are the samples, and the orange lines correspond to intervals of the heading angles.

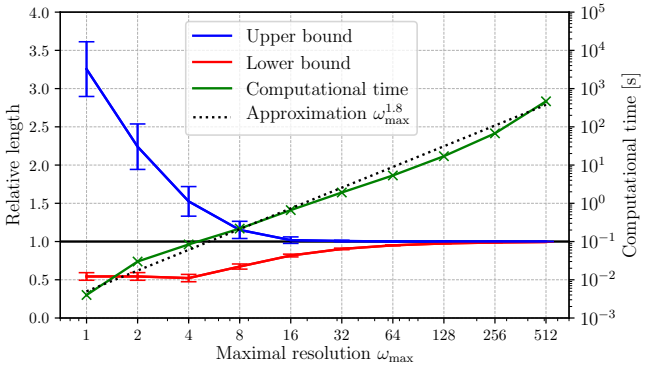

Fig. 14 Convergence of the solution cost to the lower bound and the required computational time for increasing $\omega_{\max}$. The solution cost is normalized by the best-found solution. The presented results are average values of 20 random problem instances for $n = 10$ target regions. The resolution and computational time are presented in logarithmic scales.

been determined by the optimal solution of the corresponding Euclidean TSP for the centers of the regions that have been found by the Concorde solver (Applegate et al., 2003). An example of the problem instance and its solution is depicted in Fig. 13. The instances have been used to study the convergence of the DTRP solution to the lower bound and evolution of the optimality gap.

The convergence of the DTRP solution to the lower bound has been studied for the increasing maximal resolution $\omega_{\max}$. The achieved results are depicted in Fig. 14, where the solution cost is normalized to the best-known solution of the particular problem instance. Based on the presented results, the computational time can be approximated by $\mathcal{O}(n\omega_{\max}^{1.8})$ which is mainly because of informed sampling of the regions and heading intervals.

An evolution of the relative optimality gap between the lower bound and the feasible solution cost in the above described random DTRP instances is shown in Fig. 15, where Δ is the relative gap between the lower and upper bound

$$\Delta = 1 - \frac{\mathcal{L}_L}{\mathcal{L}_U}. \tag{35}$$

The results indicate the solution of problems with $n = 100$ target regions and the optimality gap around 1% can be found in 100 seconds, which further support the hypothesis that the computational time is approximately linear with the problem size n.

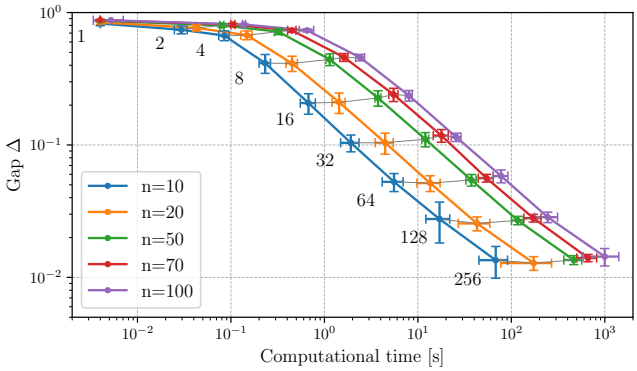

Fig. 15 The optimality gap Δ of the lower bound solution and feasible solution for problems with n target regions according to the real required computational time. The presented results are average values of 20 random problem instances, and the results are presented in logarithmic scales.

8 Conclusion

In this paper, we introduce the Generalized Dubins Interval Problem (GDIP) and provides its optimal solution based on the transformation of the GDIP to the OS-GDIP. Both forward and backward transformations are provided together with proofs of their correctness. Moreover, the benefits of the GDIP to the solution of the DTRP (a variant of the DTSPN with the prescribed sequence of the visits) are demonstrated by providing a tight lower bound of the solution cost in the sampling-based solution of the DTRP that is employed in the informed sampling. Besides, the provided lower bound allows determining the solution quality of the DTRP as the estimated optimality gap. The reported results indicate it is possible to find a solution of the DTRP with ten overlapping disk regions and the solution quality around 1% from the optimum in less than 10 seconds using a single core of a conventional processor.

A Appendix

The Dubins Interval Problem (DIP) was initially proposed and solved by Manyam et al. (2017), and the authors provided a list of all possible optimal solutions that are summarized in Table 1. The authors considered originally $\mathrm{R}_\psi\mathrm{L}_\psi$ and $\mathrm{L}_\psi\mathrm{R}_\psi$ maneuver types to be the candidates to the optimal solution of the DIP, but claim here that these types are not local minima. Although it does not affect the enumeration of possible cases, we consider it important because we can exclude these two types in the proposed optimal solution of the GDIP. Therefore, a formal proof of the following lemma is provided.

Lemma 11 *A maneuver of the $C_\psi\overline{C}_\psi$ type with two equally long turns cannot be an optimal solution of the DIP if heading angles θ_1, θ_2 remains unbounded, i.e., $\theta_1 \in \Theta_1 \setminus \{\theta_1^{min}, \theta_1^{max}\}$, $\theta_2 \in \Theta_2 \setminus \{\theta_2^{min}, \theta_2^{max}\}$.*

Proof Let us consider an $\mathrm{R}_\psi\mathrm{L}_\psi$ maneuver with two equally long turns with origins o_1 and o_2 and corresponding turn angles $\alpha, \beta \in (\pi, 2\pi)$, where w.l.o.g., we assume the minimum turning radius $\rho = 1$ for simplicity and better readability. The distance between the maneuver endpoints is denoted $l = \|p_1 - p_2\|$ and both θ_1 and θ_2 are not bounded by Θ_1 and Θ_2, respectively, see Fig. 16.

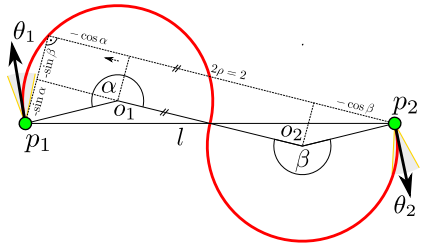

Fig. 16 $\mathrm{R}_\psi\overline{\mathrm{L}}_\psi$ maneuver of the $\mathrm{C}_\psi\overline{\mathrm{C}}_\psi$ type as a candidate solution for the DIP.

To prove the $\mathrm{R}_\psi\overline{\mathrm{L}}_\psi$ maneuver is not a candidate solution, the problem is considered as a constrained optimization of the trajectory length

$$f(\alpha, \beta) = \mathcal{L}_{\mathrm{C}_\psi\overline{\mathrm{C}}_\psi} = \alpha + \beta. \tag{36}$$

The geometrical constraint is constructed for the distance between the endpoints (see Fig. 16) such that

$$l^2 = (2 - \cos\alpha - \cos\beta)^2 + (\sin\alpha + \sin\beta)^2. \tag{37}$$

The constraint is encoded into a function $g(a, b)$ that equals to zero, i.e., $g(\alpha, \beta) = 0$, that can be expressed as

$$g(\alpha, \beta) = 3 - \frac{l^2}{2} - 2(\cos\alpha + \cos\beta) + \cos\alpha\cos\beta + \\ + \sin\alpha\sin\beta. \tag{38}$$

Local extremes can be identified using Lagrangian defined by the functions f, g, and the Lagrange multiplier λ (Bertsekas, 2014)

$$L(\alpha, \beta, \lambda) = f(\alpha, \beta) + \lambda g(\alpha, \beta). \tag{39}$$

The necessary condition for a critical point $\nabla_{\alpha,\beta,\lambda} L = 0$ holds for the case $\alpha = \beta$, but the point can be a local minimum, local maximum, or a saddle point. The second partial derivative test is utilized to distinguish these three cases. First, Lagrange multiplier λ is determined based on

$$\lambda = -\frac{\partial f}{\partial \alpha}\left(\frac{\partial g}{\partial \alpha}\right)^{-1} = -\frac{\partial f}{\partial \beta}\left(\frac{\partial g}{\partial \beta}\right)^{-1}, \tag{40}$$

and its value for the specific case when $\alpha = \beta$ is

$$\lambda|_{\alpha=\beta} = \frac{-1}{2\sin\alpha}. \tag{41}$$

The second partial derivative test is based on the Hessian $\tilde{H}$ of the Lagrangian function, also called bordered Hessian in the literature

$$\tilde{H} = \nabla^2_{\alpha,\beta,\lambda} L = \begin{bmatrix} \frac{\partial^2 L}{\partial a^2} & \frac{\partial^2 L}{\partial a \partial b} & \frac{\partial g}{\partial a} \\ \frac{\partial^2 L}{\partial b \partial a} & \frac{\partial^2 L}{\partial b^2} & \frac{\partial g}{\partial b} \\ \frac{\partial g}{\partial a} & \frac{\partial g}{\partial b} & 0 \end{bmatrix}. \tag{42}$$

The elements of bordered Hessians for the case $\alpha = \beta$ are

$$\left.\frac{\partial^2 L}{\partial \alpha^2}\right|_{\alpha=\beta} = \left.\frac{\partial^2 L}{\partial \beta^2}\right|_{\alpha=\beta} = \lambda(2\cos\alpha - 1), \tag{43}$$

$$\left.\frac{\partial^2 L}{\partial \alpha \partial \beta}\right|_{\alpha=\beta} = \lambda, \tag{44}$$

$$\left.\frac{\partial g}{\partial \alpha}\right|_{\alpha=\beta} = \left.\frac{\partial g}{\partial \beta}\right|_{\alpha=\beta} = 2\sin\alpha. \tag{45}$$

The second partial derivative test states that a point is a local maximum of function $f(\alpha, \beta)$ alongside $g(\alpha, \beta) = 0$ if $(-1)^k \det(\tilde{H}) < 0$, where $k = 1$ stands for the number of constraints. The determinant for $\alpha = \beta$

$$\det\left(\left.\tilde{H}\right|_{\alpha=\beta}\right) = 16\lambda \overbrace{(1-\cos\alpha)}^{\geq 0} \overbrace{(\sin\alpha)^2}^{\geq 0} \tag{46}$$

is positive for $\alpha \in (\pi, 2\pi)$ based on (41). Therefore, the case $\alpha = \beta$ is a local maximum and the trajectory length can be shorten by a changing $\theta_1 \in \Theta_1$ and $\theta_2 \in \Theta_2$ angles if the angles are not bounded by Θ_1 and Θ_2. The proof for $\mathrm{L}_\psi\mathrm{R}_\psi$ is analogous. □

Since $\mathrm{C}_\psi\overline{\mathrm{C}}_\psi$ maneuver type can be optimal only if at least one of the angles need to be bounded, i.e., $\theta_1 \in \{\theta_1^{\min}, \theta_1^{\max}\}$, $\theta_2 \in \{\theta_2^{\min}, \theta_2^{\max}\}$. Therefore, this type can be seen as a particular case of $\mathrm{C}\overline{\mathrm{C}}_{\boldsymbol{\psi}}$ for which both turns are larger than π, and at least one angle is constrained, see Table 1.

Acknowledgements The previous version of this paper has been presented at the Robotics: Science and Systems (RSS) 2018 conference, where it has been awarded the Best Student Paper Award Finalist.

References

Applegate D, Bixby R, Chvátal V, Cook W, Espioza D, Goycoolea M, Helsgaun K (2003) Concorde TSP Solver. URL `https://www.tsp.gatech.edu/concorde.html`, [cited: July 2, 2019]

Bertsekas DP (2014) Constrained optimization and Lagrange multiplier methods. Academic press, DOI 10.1016/C2013-0-10366-2

Bui XN, Boissonnat JD, Soueres P, Laumond JP (1994) Shortest path synthesis for Dubins non-holonomic robot. In: IEEE International Conference on Robotics and Automation (ICRA), DOI 10.1109/ROBOT.1994.351019

Cohen I, Epstein C, Shima T (2017) On the discretized Dubins Traveling Salesman Problem. IISE Transactions 49(2):238–254, DOI 10.1080/0740817X.2016.1217101

Dubins LE (1957) On curves of minimal length with a constraint on average curvature, and with prescribed initial and terminal positions and tangents. American Journal of Mathematics pp 497–516, DOI 10.2307/2372560

Faigl J, Váňa P, Saska M, Báča T, Spurný V (2017) On solution of the Dubins touring problem. In: European Conference on Mobile Robots (ECMR), IEEE, pp 1–6, DOI 10.1109/ECMR.2017.8098685

Goaoc X, Kim HS, Lazard S (2013) Bounded-curvature shortest paths through a sequence of points using convex optimization. SIAM Journal on Computing 42(2):662–684, DOI 10.1137/100816079

Isaacs JT, Klein DJ, Hespanha JP (2011) Algorithms for the Traveling Salesman Problem with Neighborhoods Involving a Dubins Vehicle. In: American Control Conference, IEEE, pp 1704–1709, DOI 10.1109/ACC.2011.5991501

Le Ny J, Frazzoli E, Feron E (2007) The curvature-constrained traveling salesman problem for high point densities. In: 46th Conference on Decision and Control, IEEE, pp 5985–5990, DOI 10.1109/CDC.2007.4434503

Macharet DG, Campos MFM (2018) A survey on routing problems and robotic systems. Robotica 36(12):1–23, DOI 10.1017/S0263574718000735

Macharet DG, Neto AA, da Camara Neto VF, Campos MF (2011) Nonholonomic path planning optimization for Dubins' vehicles. In: IEEE International Conference on Robotics and Automation (ICRA), pp 4208–4213, DOI 10.1109/ICRA.2011.5980239

Manyam SG, Rathinam S (2018) On tightly bounding the dubins traveling salesman's optimum. Journal of Dynamic Systems, Measurement, and Control 140(7):071013, DOI 10.1115/1.4039099

Manyam SG, Rathinam S, Casbeer D, Garcia E (2017) Tightly Bounding the Shortest Dubins Paths Through a Sequence of Points. Journal of Intelligent & Robotic Systems pp 1–17, DOI 10.1007/s10846-016-0459-4

Oberlin P, Rathinam S, Darbha S (2010) Today's Traveling Salesman Problem. IEEE Robotics & Automation Magazine 17(4):70–77, DOI 10.1109/MRA.2010.938844

Obermeyer KJ (2009) Path planning for a UAV performing reconnaissance of static ground targets in terrain. In: AIAA Guidance, Navigation, and Control Conference, pp 10–13, DOI 10.2514/6.2009-5888

Pěnička R, Faigl J, Váňa P, Saska M (2017) Dubins Orienteering Problem. Robotics and Automation Letters 2(2):1210–1217, DOI 10.1109/LRA.2017.2666261

Savla K, Frazzoli E, Bullo F (2005) On the point-to-point and traveling salesperson problems for Dubins' vehicle. In: American Control Conference, IEEE, pp 786–791, DOI 10.1109/ACC.2005.1470055

Yu X, Hung J (2012) Optimal path planning for an autonomous robot-trailer system. In: Industrial Electronics Society, 38th Annual Conference on (IECON), IEEE, pp 2762–2767, DOI 10.1109/IECON.2012.6389140